



Satchwell, T., & Toye, A. (2016). A new junctional hierarchy. *Blood*, 128(1), 11-12. <https://doi.org/10.1182/blood-2016-05-711788>

Peer reviewed version

Link to published version (if available):
[10.1182/blood-2016-05-711788](https://doi.org/10.1182/blood-2016-05-711788)

[Link to publication record in Explore Bristol Research](#)
PDF-document

This is the accepted author manuscript (AAM). The final published version (version of record) is available online via American Society of Hematology at <http://dx.doi.org/10.1182/blood-2016-05-711788>. Please refer to any applicable terms of use of the publisher.

University of Bristol - Explore Bristol Research

General rights

This document is made available in accordance with publisher policies. Please cite only the published version using the reference above. Full terms of use are available:
<http://www.bristol.ac.uk/red/research-policy/pure/user-guides/ebr-terms/>

Laser Ablation – Accelerator Mass Spectrometry: a novel approach for rapid radiocarbon analyses of carbonate archives at high spatial resolution

Caroline Welte^{1,2}, Lukas Wacker², Bodo Hattendorf¹, Marcus Christl², Christiane Yeman², Jens Fohlmeister³, Sebastian F.M. Breitenbach⁴, Laura F. Robinson⁵, Allen H. Andrews⁶, André Freiwald⁷, Jesse R. Farmer⁸, Hans-Arno Synal², Detlef Günther¹

¹ Laboratory of Inorganic Chemistry, D-CHAB, ETHZ, Vladimir-Prelog Weg 1, 8093 Zurich, Switzerland

² Laboratory of Ion Beam Physics, ETHZ, Otto-Stern Weg 5, HPK, 8093 Zurich, Switzerland

³ Institute for Environmental Physics, University of Heidelberg, Germany

⁴ Institute of Geology, Mineralogy and Geophysics, Ruhr-University Bochum, Bochum, Germany

⁵ School of Earth Sciences, University of Bristol, UK

⁶ NOAA Fisheries, Pacific Islands Fisheries Science Center, USA

⁷ Senckenberg am Meer, Abteilung Meeresforschung, Wilhelmshaven, Germany

⁸ Earth and Environmental Sciences and Lamont-Doherty Earth Observatory of Columbia University, New York, USA

Keywords: Radiocarbon, Laser Ablation, Accelerator Mass Spectrometry, Carbonate record, bomb peak

Abstract

A new instrumental setup, combining laser ablation (LA) with accelerator mass spectrometry (AMS), has been investigated for the online radiocarbon (¹⁴C) analysis of carbonate records. Samples were placed in an in-house designed LA-cell and CO₂ gas was produced by ablation using a 193 nm ArF excimer laser. The ¹⁴C/¹²C abundance ratio of the gas was then analyzed by gas ion source AMS. This configuration allows flexible and time resolved acquisition of ¹⁴C profiles in contrast to conventional measurements, where only the bulk composition of discrete samples can be obtained. Three different measurement modes, i.e. discrete layer analysis, survey scans and precision scans, were investigated and compared using a

stalagmite sample and, subsequently, applied to terrestrial and marine carbonates. Depending on the measurement mode, a precision of typically 1-5 % combined with a spatial resolution of 100 μm can be obtained. Prominent ^{14}C features, such as the atomic bomb ^{14}C peak, can be resolved by scanning several cm of a sample within one hour. Stalagmite, deep-sea coral and mollusk shell samples yielded comparable signal intensities, which again were comparable to those of conventional gas measurements. The novel LA-AMS setup allowed rapid scans on a variety of sample materials with high spatial resolution.

1. Introduction

Carbonate radiocarbon (^{14}C) records are of great interest in a variety of research fields, such as paleoclimatology^{1,2}, establishing or improving chronologies³⁻⁵ understanding the carbon cycle^{6,7}, and age validation of marine organisms⁸. Because carbonates usually can be radiometrically dated (e.g., Uranium-Thorium (U/Th) disequilibrium methods^{9,10}), ^{14}C in stalagmites and corals provides a powerful geochemical tracer to study, for example for soil carbon dynamics¹¹⁻¹³ and/or past ocean circulation^{14,15}. In very young carbonates (<200 years) where U/Th dating becomes less precise, the detection of the atomic bomb ^{14}C peak caused by nuclear weapon tests during the 1950s and 1960s may provide indirect, stratigraphic age information^{16,17}. Either of the above applications requires access to the ^{14}C signature along the archive's growth axis at high spatial resolution, which involves the analysis of a great quantity of small subsamples. Micro-sampling for conventional ^{14}C analysis is commonly done by micromilling techniques, reaching spatial resolutions of a few dozen to hundreds of μm , but requiring an enormous work load^{11,13,18}. In addition to the tedious sampling process, the following multi-step chemical procedure (including graphitization) necessary for the ^{14}C analysis by accelerator mass spectrometry (AMS) involves the risk of sample contamination.

The coupling of laser ablation (LA) with inductively coupled plasma mass spectrometry (LA-ICPMS) is a widely used analytical technique that allows rapid analyses of solid materials at high spatial resolution, while little to no sample preparation is required¹⁹⁻²¹. To date, LA has mainly been applied to elemental and isotopic analyses of solid materials, and there are few studies that deal with ^{14}C measurements where LA is used as a sampling technique. Rosenheim, et al.²² showed that when focusing a UV laser (quintupled Nd:YAG, 213 nm) onto a carbonate sample, approximately 30 % of the ablated material was converted into CO_2 . In this pilot study, the CO_2 was converted into graphite for a conventional accelerator mass spectrometry (AMS) measurement and therefore it did not benefit from the online injection of CO_2 when using gas ion source AMS^{23,24}. Fractionation effects that may occur during the ablation event and might lead to fractionation of the C isotopes are not of concern in AMS analyses, as the internal normalization

59 using the $^{13}\text{C}/^{12}\text{C}$ ratio should also correct for mass dependent fractionation effects that occur during
60 ablation. Wacker, et al. ²⁵ performed the first direct coupling of LA with AMS using a commercial LA unit
61 (LSX 213, CETAC Technologies, Omaha, USA) and a simple LA-cell design. In the proof of principle
62 experiment they performed, the known $^{14}\text{C}/^{12}\text{C}$ ratio of a natural sample was reproduced within
63 uncertainty. Subsequently, an LA-setup with optimized cell geometry was designed^{26,27}. This novel LA-AMS
64 setup offers high flexibility regarding analysis time, spatial resolution and measurement precision.
65 Standards were reproduced within uncertainties and the blank level allows ^{14}C -measurements to ages as
66 old as 35 000 years.

67 The aim of this study was to demonstrate the applicability of the novel LA-AMS setup in the analysis of
68 natural carbonate samples. First, different laser scanning modes implemented into the new setup were
69 compared with regard to analysis time, material consumption, spatial resolution and measurement
70 precision. Second, the applicability of the system to different materials such as stalagmites, corals and
71 shells was investigated and $^{14}\text{C}/^{12}\text{C}$ data from conventional graphite AMS analysis could be reproduced
72 within the uncertainties using LA-AMS.

73

2. Methods

2.1. Instrumental Setup

An ArF excimer laser (Ex5, Argon Fluoride 193 nm, GAM LASER, Orlando, USA) operating at a wavelength of 193 nm is used to generate pulses at a repetition rate ranging from 150 - 250 Hz and a fluence between 1 and 2.5 J/cm² on the sample surface, delivered as a rectangular spot of 110 x 680 μm². The ablation process can be observed via a monochrome CCD camera (AVT MANTA G-125B, Allied Vision Technologies, Stadtroda, Germany) combined with a zoom lens (OPTO TUBUS Z-1,0/146, Opto, Gräfelfing, Germany). The ablation rate of the LA-AMS system is approximately 100 μg/min of CaCO₃ when ablating at a laser repetition rate of 200 Hz. Samples with maximum dimensions of 150 x 25 x 15 mm³ can be placed in the sample holder of an in-house designed LA-cell (Figure 1, adapted from ²⁷), which is equipped with a xy-positioning system (SLC, SmarAct GmbH, Germany) that allows precise positioning of the sample relative to the laser beam. Helium is used as a carrier gas to transport the laser-produced CO₂ from the ablation spot to the ion source via a fused silica capillary ("5" in Figure 1). The background helium pressure in the LA-cell was adjusted to provide a gas flow rate on the order of 1.5 mL/min through the capillary. A detailed description of the LA-cell and the gas handling system can be found in ²⁷.

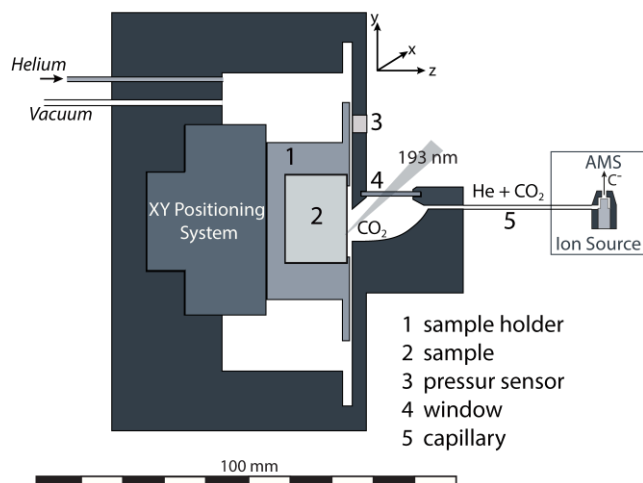


Figure 1 Schematic of the LA-AMS setup: CO₂ is produced in the ablation cell by focusing an ArF laser operating at 193 nm on the carbonate sample. The CO₂ is transported with helium as carrier gas into the gas ion source of the AMS, where negative C ions are formed and the ¹⁴C content is measured.

The ¹⁴C-measurements were performed with the ETH Zurich MIniCarbonDAtingSystem AMS system^{28,29} (MICADAS, Ionplus AG, Dietikon, Switzerland) that is routinely used for gas measurements^{23,24}. Prior to LA-AMS measurements the AMS was optimized for highest sensitivity by direct injection of a 5 % CO₂ in helium gas mixture. Subsequently, two to three conventional gas standards (NIST Ox-I or NIST Ox-II) and two to

three conventional ^{14}C blanks (5 % CO_2 in helium, Messer Schweiz AG, Lenzburg, Switzerland) were measured to ensure optimum working conditions of the MICADAS. A blank and fractionation correction was applied to the measured $^{14}\text{C}/^{12}\text{C}$ -ratios and, subsequently, normalization to the calibration standard was performed using the data evaluation software BATS³⁰. The final data are reported as $F^{14}\text{C}$ (fraction modern), which corresponds to the activity ratio of the sample relative to a modern reference material^{10,31}. Initially, conventional OxI and OxII gas standards were used for calibration of the samples because no suitable solid standard material was available. Subsequently, a homogenized and compacted carbonate powder from a coral (CSTD)³² with a nominal $F^{14}\text{C}$ of 0.9445 ± 0.0018 was measured before and after each sample analysis and used for normalization. Details on the standards used for normalization can be found in Table 1.

2.2. Modes of measurement

Requiring only minimal sample preparation (compare ²⁷), the LA-AMS setup provides discrete data with a minimum integration time of 10 sec. The XY-positioning system in the LA-cell was controlled by an in-house implemented LabVIEW program (National Instruments, Austin, Texas, USA) and allowed precise movement of the sample relative to the laser beam. Three contrasting sampling strategies (Modes 1-3) were developed in order to provide flexibility in adapting to the analysis purpose and the required precision (Figure 2).

- 1) **Discrete layer analyses (Mode 1, Figure 2a)** are equivalent to conventional drilling of samples by ablating material parallel to individual growth layers only (i.e. within carbonate deposits that formed at the same time). The spatial resolution along the growth axis depends on the laser beam width (i.e., 110 μm).
- 2) A **survey scan (Mode 2, Figure 2b)** allows scanning along a sample parallel to the growth direction. The spatial resolution depends on laser beam size, laser repetition rate and scan speed.
- 3) **Precision scan (Mode 3, Figure 2c)** aims for continuous sampling along the growth axis, while the sampling time within the growth layer is increased by scanning in a zig-zag pattern. Part of the scan (Δy) is performed within single growth layers, followed by a return scan with a displacement δx along the x-axis. The entire scan length along the growth axis will be denoted as Δx . In the following the parameters are reported as (Δx , Δy , δx).

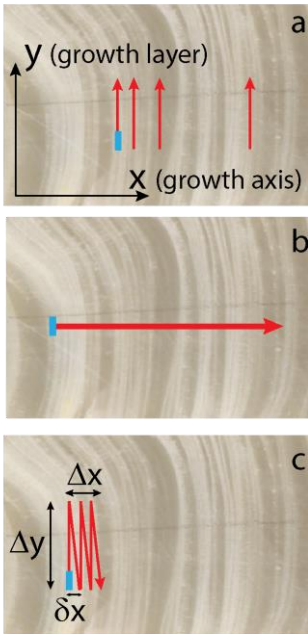


Figure 2 Comparison of the three scanning modes available for LA-AMS measurements. (a) Mode 1: Discrete layer analysis within discrete growth layers, (b) Mode 2: Survey scans parallel to the growth direction, (c) Mode 3: Precision scans. The red arrows represent the scanning direction and the blue rectangle indicates the orientation of the laser spot.

In the case of conventional ^{14}C AMS measurements, data evaluation had the following scheme: individual samples were measured and the normalized $^{14}\text{C}/^{12}\text{C}$ -ratios were integrated yielding one averaged $^{14}\text{C}/^{12}\text{C}$ ratio per sample. Hence, the data integration period was equal to the data acquisition period, which was also the case for Mode 1 in LA-AMS analysis. Modes 2 and 3 required a different data evaluation procedure: the $^{14}\text{C}/^{12}\text{C}$ -ratio continuously changes as the laser scans across different growth layers of the carbonate record and depending on the measurement time one or more sputter targets of the gas ion source were used. This offered the greatest flexibility concerning data evaluation, such as the data integration periods; hence, spatial resolution and measurement precision could be selected according to the needs of the application after the analysis. Thus, by integrating fewer or more data points along the scan pathway, the measurement precision can be adjusted.

2.3. Samples

Fast to slow growing stalagmites and biogenic carbonates (corals, shells) were used in this study (Table 1). Samples were selected according to their (i) ^{14}C signal sequence, i.e. whether they exhibit a distinct signal

such as the bomb peak, (ii) the magnitude of the signal rise, and (iii) the spatial expansion of the signal in the sample (detailed information can be found in the SI).

Table 1 Overview of the different samples and sample materials as well as their expected and LA-AMS derived $F^{14}C$ (fraction modern).

Sample label	Type of sample	mineral	Growth rate ($\mu\text{m/a}$)	Known $F^{14}C$	Measured $F^{14}C$ (LA-AMS, this study)
ER-77	stalagmite	calcite	120	$0.88 - 1.19^{13}$	$0.81 - 1.30^a$
BU-4	stalagmite	calcite	30-50	$0.88 - 1.00^{33}$	$0.82 - 1.04^a$
SOP-20	stalagmite	calcite	3-15		$0.03 - 0.77^a$
BS_1299m	coral	calcite	35-75	$0.92 - 0.98^{34}$	$0.90 - 1.00^a$
Oyster PH3-A	mollusk	aragonite		$1.11 - 1.15^*$	$1.09 - 1.22^b$
Arctica islandica	mollusk	aragonite		$0.925 \pm 0.002^*$	$0.88 - 0.92^b$

*this work; ^anormalized to OxII, ^bnormalized to CSTD

3. Results and Discussion

3.1. Applying the three scanning modes

Stalagmite ER-77 was considered “ideal” for comparing the scanning modes due to its distinct ^{14}C profile and high growth rate ($120 \mu\text{m/a}$). It exhibits a pronounced ^{14}C bomb-peak with an $F^{14}C$ increase of 0.3 within several mm. Conventional sampling had been performed at the center of the stalagmite’s growth axis with a spatial resolution of 0.6 mm per subsample ¹³. The bomb peak expands across the six topmost samples covering a width of ca. 4 mm (Figure 3). The three LA-AMS scanning modes were performed with different offsets to the growth axis: the precision scan (Mode 3) was placed closest to the growth axis covering an effective distance of 3 mm. Discrete layer analysis (Mode 1) covering 4 mm and the survey scan (Mode 2) covering 2.5 mm were performed with increasing distance from the growth axis (detailed information can be found in the SI).

3.1.1. Discrete layer analyses (Mode 1)

Nine discrete scans were made, each covering a length of 2–2.6 mm. The scan velocity was set between 2.5 and 5 $\mu\text{m/s}$ and the spacing between the individual scans covered 300 μm for the seven topmost

samples and 1 mm for the two lower ones. The $^{14}\text{C}/^{12}\text{C}$ raw data (blue dots) of the nine sub-scans are depicted in Figure 3 a, with the onset of the bomb peak found within 60 minutes of analysis. Horizontal red bars indicate the lifetime of a sputter target and represent the period of continuous data acquisition. The vertical dashed and horizontal black lines represent the “data integration period”, which is equal to the “data acquisition period” in the case of “Mode 1.” Integrated, background corrected and normalized data are depicted in Figure 3 b, where red circles represent the LA-data and black squares the conventional measurements. For LA-AMS a measurement precision on the order of 2% is achieved corresponding to the uncertainty from counting statistics and the spatial resolution, defined by the crater width, is 110 μm . The material consumption lies between 1 – 1.5 mg per subsample and the measurement time per aliquot ranges from 8 – 15 min, resulting in ca. 2 hours total analysis time. The LA-derived data match the conventionally derived $F^{14}\text{C}$ values very well and within the statistical uncertainties, as confirmed by a χ^2 -test (95% confidence limit). Since the spacing between individual scans was not minimal, there is capacity for placing two to three additional subsamples between the topmost seven samples and up to nine between the two lower ones.

3.1.2. Survey scan (Mode 2)

A survey scan across the top 2.5 mm of the stalagmite was performed with a scan velocity of 2.5 $\mu\text{m}/\text{s}$ resulting in an overall measurement time of 17 minutes. The $^{14}\text{C}/^{12}\text{C}$ ratios are shown as blue dots in Figure 3 c. The scan was performed on one sputter target and data integrated for 60 sec, or a span (Δx) of 150 μm respectively. The resulting $F^{14}\text{C}$ is represented by the red circles in Figure 3 d. The survey scan was performed within less than 20 minutes, yielding a precision on the order of 4% for each aliquot and a spatial resolution of ca. 260 μm . 1.6 mg of CaCO_3 were consumed for the entire scan corresponding to 0.1 mg per integration period. A χ^2 -test was performed to test the agreement between LA and conventional data within a 95% confidence limit. When the LA-data is shifted by a $F^{14}\text{C}$ 0.03 to higher values, the χ^2 -test yields good agreement between the two data sets. This offset of the data is discussed in Section 3.3. The LA-scan was performed with an offset of approximately ca. 1 cm relative to the stalagmite growth axis. The growth layer structure at this region is different to that at the center of the stalagmite as growth layers thin out and start to slope with increasing distance from the center. Thus, the bomb peak is found in the upper 2.5 mm instead of the upper 4 mm, as found with conventional analysis, where samples were taken at the stalagmite’s growth axis.

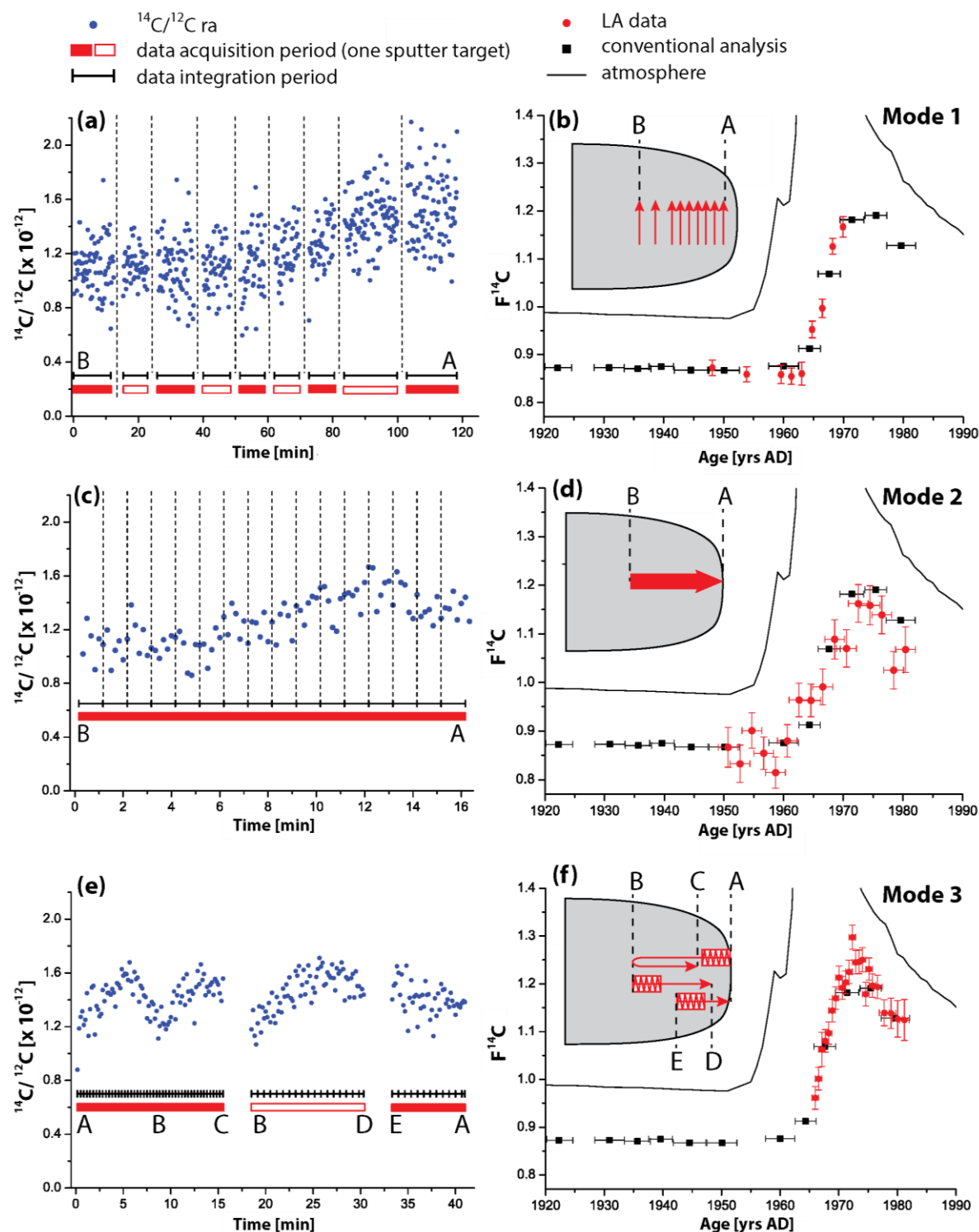


Figure 3 Comparison of the three measurement modes using stalagmite ER-77: (a) and (b) discrete layer analyses, (c) and (d) survey scan, (e) and (f) precision scan. In the left part of the figure corrected $^{14}\text{C}/^{12}\text{C}$ -ratios are plotted against the acquisition time. Red bars (open and solid) correspond to one sputter target and black bars/vertical dashed lines to the integration time. In the right part of the figure, the integrated $F^{14}\text{C}$ values are shown and the inserts indicate the path of the scan (not to scale).

3.1.3. Precision scan (Mode 3)

Three precision scans were performed within the top 3 mm of stalagmite ER-77. The velocity was set to 200 $\mu\text{m/s}$ for the first scan, allowing scanning back and forth while using a single sputter target. The scan parameters were $\Delta x = 3 \text{ mm}$, $\Delta y = 2 \text{ mm}$, $\delta x = 100 \mu\text{m}$. A second and third scan stacked on the track of the first one, this time facing towards the top, were performed with a scan velocity of 100 $\mu\text{m/s}$, while all other parameters were kept constant. The scanning paths are shown in the inset of Figure 3 (f) and are reflected in the $^{14}\text{C}/^{12}\text{C}$ raw data (blue circles in Figure 3 e). The two peaks on the first sputter target correspond to the back and forth movement across the bomb peak in the sample. The second and third scan were performed with two sputter targets. They overlap at the transition and the bomb peak was crossed only once. The integration time is 60 s, which equals the duration of one zig-zag step (compare black horizontal bars in Figure 3 e) and corresponds to a material consumption of 130 $\mu\text{g CaCO}_3$. The average $F^{14}\text{C}$ of the three scans was calculated (red squares in Figure 3 f) and, since the signal intensity at the top of the sample was much lower than for the other samples, the mean of two zig-zag steps was taken for the topmost four data points. The spatial resolution is 300 μm compared to 200 μm achieved for the other subsamples. A measurement precision on the order of 2% is obtained, except for the four data points at the top, for which 4% was achieved. The overall measurement time was 40 minutes.

3.1.4. Comparison of the three LA-AMS scanning modes

Each of the presented scanning modes has certain strengths with regard to measurement time, achievable precision, spatial resolution and sample consumption. Spatial resolution and measurement precision depend on the scan velocity, laser parameters and the efficiency of the setup. The major advantage of the three measurement modes, when compared to conventional methods, is the shorter analysis time, and thus sample throughput. This is especially true for the survey scan (Mode 2), which allows analyzing a comparably large section of the sample (i.e., several centimeters within one hour). A quick overview of the ^{14}C -content across a carbonate record can be established using Mode 2 and subsequently a precision scan (Mode 3) at selected regions can be performed to achieve higher measurement precisions. Ablating across different growth layers is only desired in the case of survey scans. For discrete layer analysis (Mode 1) and precision scans (Mode 3) material is collected within individual growth layers. Since the laser beam is a rectangular shape, the maximum scanning distance within each growth layer is limited by the region of parallel growth in the sample and with respect to the laser spot geometry. This could be improved by using a smaller, quadratic or circular laser spot at the expense of CO_2 production. To achieve higher precision at

a smaller spot size, signal intensities obtained with the LA-AMS setup need to be improved and is the subject of future studies.

With the three measurement modes, the ^{14}C signal in stalagmite ER-77 was reproduced within the statistical uncertainties. The precision scan revealed that bomb ^{14}C reaches $F^{14}\text{C}$ levels of up to 1.30, whereas conventional data suggested that the peak was at approximately 1.20. This highlights the enormous potential of this novel method because of the increased resolution. The key findings for all three LA-AMS scanning modes and the conventional AMS measurements are summarized in Table 2.

Table 2 Comparison of the three LA-measurement modes with conventional graphite-AMS measurements of ER-77.

Measurement mode	time/data point (min)	spatial resolution (μm)	material consumption (mg CaCO_3)	measurement precision (%)
micromill and conventional graphite	60	≥ 400	8	0.4
LA – discrete layer	10	100 – 200	1 – 1.5	1 – 2
LA - survey scan	0.5 – 2	300 – 1700	0.1 – 0.2	4 – 6
LA – precision scan	0.5 – 4	200 – 1000	0.1 – 0.4	2 – 4

3.2. Potential of LA-AMS for stalagmites, corals and other marine carbonates

LA-AMS analysis bears enormous potential for the analysis of carbonate archives. Reconnaissance scanning allows rapid identification of the potential of a given sample, thus reducing analysis time and effective costs. In many cases, the ^{14}C -variability is not as pronounced as observed in stalagmite ER-77. In the following section, the potential of the LA-AMS setup for samples with smaller variations in their ^{14}C content, as well as for other carbonate materials is addressed. First, a slow growing stalagmite will be investigated that exhibits an attenuated bomb peak. Second, a stalagmite record is analyzed that exhibits a growth interruption of more than 350 ka. Finally, the LA-AMS setup will be used to investigate a deep-sea coral sample exhibiting a bomb ^{14}C peak, and its potential for use on aragonite shell samples.

3.2.1. Attenuated bomb ^{14}C peak in a stalagmite (BU-4)

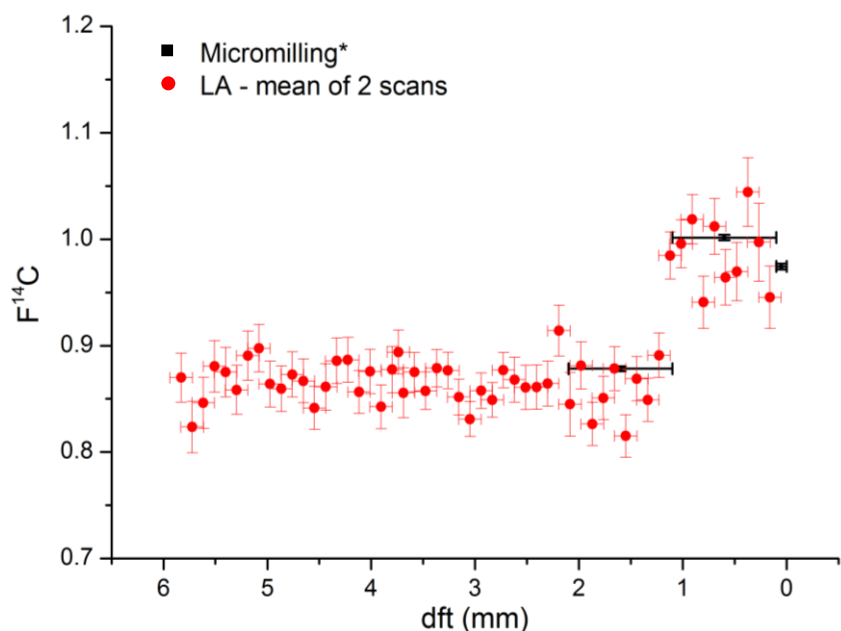


Figure 4 LA-AMS data (red circles) compared to conventionally derived solid AMS measurements (black squares). The high resolution achieved with LA-AMS allows identification of the abrupt onset of the bomb peak in the upper-most mm of the stalagmite sample.

Two precision scans were performed in opposite directions within the top 6 mm of the slow growing stalagmite BU-4. Conventionally obtained and LA-AMS derived data match well within the statistical uncertainties (Figure 4). The abrupt onset of the bomb peak was revealed, even though it covered a $F^{14}\text{C}$ rise of only 0.12 and is located within the uppermost millimeter of the stalagmite (detailed information can be found in the SI). A χ^2 test was performed confirming that the LA and conventional data are not significantly different (95% confidence limit).

3.2.2. Growth interruption in a stalagmite (SOP-20)

Scans in Mode 2 and 3 were performed on all three sections of the Siberian sample. The results for the upper sections can be found in the SI. Two survey scans facing in opposite direction were performed on SOP-20-bottom. Both scans exhibit a clear step in $F^{14}\text{C}$ caused by a growth interruption at approximately 55 to 56 mm (Figure 5). Assuming an ideal step between the ^{14}C -dead (> 55.5 mm, see Section 1c in SI for details) and ^{14}C -containing (<55.5 mm) sections, carry-over effects and washout of the laser system can be studied. Based on the comparison of both scans, a washout time of approximately 10 sec was estimated.

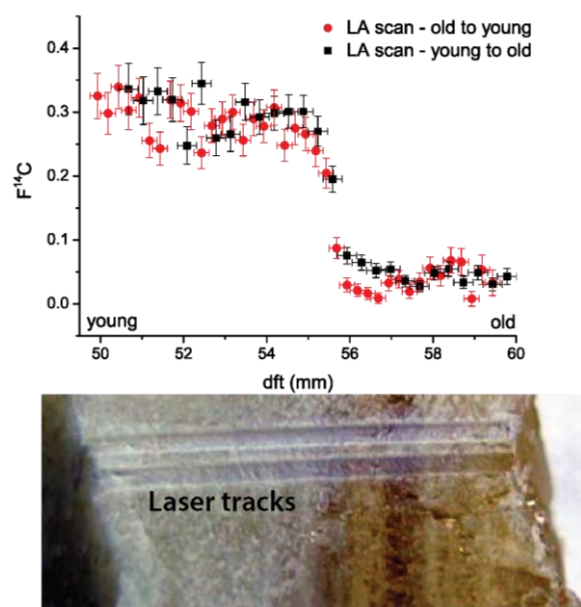


Figure 5 Two survey scans were performed on the bottom part of stalagmite SOP-20 confirming the growth interruption identified by U-Th ages of 8.711 ± 0.012 ka BP and 377 ± 7 ka BP. (DFT: distance from top).

3.2.3. Other samples

To further exemplify the potential of the new LA-AMS method, a calcitic bamboo coral (*Keratoisis* sp. sample BS_1299m³⁴) was analyzed using the precision scan (Mode 3). At the outer edge of the sample the bomb peak with an $F^{14}C$ increase of 0.06 was found, which is in agreement with the conventional data (compare Section 2 c and Figure 4 in SI).

Two stacked precision scans were performed in opposite directions on a sectioned shell from a black-lip pearl oyster (*Pinctada margaritifera*) from the Hawaiian Islands. Comparison of LA-AMS and conventional ^{14}C data from a series of micromill extractions (both within the shell and from a regional hermatypic coral record) showed good agreement within the statistical uncertainties (compare Section 2 d and Figure 5 in SI).

One survey scan was performed on another shell sample from a long-lived species, *Arctica islandica*, found on the beach of Fur, Denmark. Within the topmost 30 mm a $F^{14}C$ of 0.92 ± 0.01 was measured, while the average value of the older part was lower with an $F^{14}C$ value of 0.88 ± 0.02 . The LA-data was confirmed by one conventional graphite sample that was in agreement. The sample was taken at the youngest part of the shell and yielded a $F^{14}C$ of 0.925 ± 0.002 . In contrast to the initial assumption that this shell contained

the bomb peak, the LA-AMS analyses revealed within less than one hour, that the shell was much older (compare Section 2 e and Figure 6 in SI).

3.3. Potential and limits of LA-AMS

The applicability of the novel LA-AMS technique for ^{14}C analyses of various carbonate archives and its potential with regard to spatial resolution and measurement precision has been exemplified with the above described samples. Signal intensities obtained for aragonite and calcite samples were on the same order of magnitude and comparable to ion currents reached for conventional gas measurements. The major advantages of the novel technique are short measurement times and its high spatial resolution. LA-AMS is especially useful for the rapid identification of pronounced ^{14}C signatures, such as the ^{14}C bomb peak or a growth interruption. A major drawback is the measurement precision, which is worsened by a factor of two or even higher compared with conventional graphite analyses. χ^2 tests were performed to confirm the agreement between LA-derived $F^{14}\text{C}$ data of samples with conventional data. For samples where external standard gas was used for calibration (compare Table 1), the χ^2 test verified the compliance either directly, or after applying an $F^{14}\text{C}$ offset correction between 0.02 – 0.03. The offset is most likely caused by the calibration method, because in this case a standard gas was used, which is introduced into the AMS directly from the gas cylinder. It is still a matter of investigation to identify the origin of the offset. One sample was normalized using the LA-AMS standard CSTD. Even though, the LA-derived data reflects the trend of the conventional data, in this case, the χ^2 test did not confirm that LA-derived and conventional data matched within the 95% confidence interval, not even after performing offset corrections. During the analyses of this sample, exceptionally high background on ^{14}C caused by broken up molecules was observed (see Section 2 c in SI), which is most likely the reason for the discrepancy between LA.

For each analyzed sample, the ^{14}C range obtained by LA-AMS was larger than in the case of the conventional analyses (Table 1). Due to the higher spatial resolution achieved with LA-AMS, more detailed insight in the ^{14}C -content within the carbonate record can be gained.

4. Conclusion

The LA-AMS technique was successfully applied to ^{14}C analyses of carbonate archives including stalagmites, deep-sea coral and mollusk shells. Different sampling strategies were compared with regard to

measurement precision, spatial resolution, analysis time and material consumption. LA-AMS samples required between 0.05 to 1.5 mg of CaCO_3 with measurement times ranging from 1 to 10 minutes, whereby a precision of 1 to 6 % and a spatial resolution between 100 and 1700 μm were reached. The different scanning modes complement each other and can be combined in order to yield optimal results which may depend on the focus of the study. Continuous scanning provides great flexibility with regard to measurement precision and spatial resolution. Studies with a limited amount of sample can profit from this new technique because comparably only a small amount of material is consumed. A major advantage of LA-AMS is the exceptional sample throughput that allows a rapid assessment of ^{14}C content on a large number of subsamples. Nevertheless, it is desirable to further increase the measurement precision in order to resolve less pronounced ^{14}C signals. Improving the overall efficiency with a modified LA-cell design and an optimized optical setup would allow for a reduction of the scanning velocity, which would increase the analysis time and consequently improve the counting statistics to close the gap in measurement precision between analysis using LA-AMS compared to conventional gas and graphite analysis. A modification of the cell design and the beam transportation system would also provide an opportunity to operate at higher laser fluences. These improvements of the LA-AMS technique will allow establishing ^{14}C profiles of carbonate archives with high precision and unprecedented spatial resolution at an exceptionally high sample throughput.

Acknowledgements

Financial support was given by ETH (Research Grant ETH-11 11-1) and is gratefully acknowledged. We thank Philip Trüssel for the technical support as well as Silvia Frisia, Anton Vaks and Gideon M. Henderson for providing sample material. We also thank the reviewers who helped to improve this manuscript.

338

- 339 (1) Mangini, A.; Lomitschka, M.; Eichstadter, R.; Frank, N.; Vogler, S.; Bonani, G.; Hajdas, I.; Patzold, J.
340 *Nature* **1998**, *392*, 347-348.
- 341 (2) Fleitmann, D.; Burns, S. J.; Mudelsee, M.; Neff, U.; Kramers, J.; Mangini, A.; Matter, A. *Science* **2003**,
342 *300*, 1737-1739.
- 343 (3) Reimer, P. J.; Baillie, M. G. L.; Bard, E.; Bayliss, A.; Beck, W.; Bertrand, C. J. H.; Blackwell, P. G.; Buck, C.
344 E.; Burr, G. S.; Cutler, K. B.; Damon, P. E.; Edwards, R. L.; Fairbanks, R. G.; Friedrich, M.; Guilderson, T. P.;
345 Hogg, A. G.; Hughen, K. A.; Kromer, B.; McCormac, G.; Manning, S.; Ramsey, C. B.; Reimer, R. W.; Remmele,
346 S.; Southon, J. R.; Stuiver, M.; Talamo, S.; Taylor, F. W.; van der Plicht, J.; Weyhenmeyer, C. E. *Radiocarbon*
347 **2004**, *46*, 1029-1058.
- 348 (4) Hoffmann, D. L.; Beck, J. W.; Richards, D. A.; Smart, P. L.; Singarayer, J. S.; Ketchmark, T.; Hawkesworth,
349 C. J. *Earth and Planetary Science Letters* **2010**, *289*, 1-10.
- 350 (5) Ridley, H. E.; Asmerom, Y.; Baldini, J. U. L.; Breitenbach, S. F. M.; Aquino, V. V.; Prufer, K. M.; Culleton,
351 B. J.; Polyak, V.; Lechleitner, F. A.; Kennett, D. J.; Zhang, M. H.; Marwan, N.; Macpherson, C. G.; Baldini, L.
352 M.; Xiao, T. Y.; Peterkin, J. L.; Awe, J.; Haug, G. H. *Nat. Geosci.* **2015**, *8*, 195-200.
- 353 (6) Druffel, E. R.; Griffin, M. S.; Beaupre, S. R.; Dunbar, R. B. *Geophys. Res. Lett.* **2007**, *34*, L09601.
- 354 (7) Robinson, L. F.; Adkins, J. F.; Keigwin, L. D.; Southon, J.; Fernandez, D. P.; Wang, S. L.; Scheirer, D. S.
355 *Science* **2005**, *310*(5753), 1469-1473.
- 356 (8) Andrews, A. H.; Barnett, B. K.; Allman, R. J.; Moyer, R. P.; Trowbridge, H. D. *Can. J. Fish. Aquat. Sci.* **2013**,
357 *70*, 1131-1140.
- 358 (9) Scholz, D.; Hoffmann, D. *Quater. Sci. J.* **2008**, *57*, 52-77.
- 359 (10) Edwards, R. L.; Gallup, C. D.; Cheng, H. *Uranium-Series Geochemistry* **2003**, *52*, 363-405.
- 360 (11) Rudzka-Phillips, D.; McDermott, F.; Jackson, A.; Fleitmann, D. *Geochimica et Cosmochimica Acta* **2013**,
361 *112*, 32-51.
- 362 (12) Genty, D.; Vokal, B.; Obelich, B.; Massault, M. *Earth Planet. Sci. Lett.* **1998**, *160*, 795-809.
- 363 (13) Fohlmeister, J.; Kromer, B.; Mangini, A. *Radiocarbon* **2011**, *53*, 99-115.
- 364 (14) Adkins, J. F.; Cheng, H.; Boyle, E. A.; Druffel, E. R. M.; Edwards, R. L. *Science* **1998**, *280*, 725-728.
- 365 (15) Frank, N.; Paterne, M.; Ayliffe, L.; van Weering, T.; Henriot, J. P.; Blamart, D. *Earth Planet. Sci. Lett.*
366 **2004**, *219*, 297-309.
- 367 (16) Hodge, E.; McDonald, J.; Fischer, M.; Redwood, D.; Hua, Q.; Levchenko, V.; Drysdale, R.; Waring, C.;
368 Fink, D. *Radiocarbon* **2011**, *53*, 345-357.
- 369 (17) Hua, Q.; McDonald, J.; Redwood, D.; Drysdale, R.; Lee, S.; Fallon, S.; Hellstrom, J. *Quat. Geochronol.*
370 **2012**, *14*, 67-80.
- 371 (18) Noronha, A. L.; Johnson, K. R.; Southon, J. R.; Hu, C. Y.; Ruan, J. Y.; McCabe-Glynn, S. *Quaternary*
372 *Science Reviews* **2015**, *127*, 37-47.
- 373 (19) Gray, A. L. *Analyst* **1985**, *110*, 551-556.
- 374 (20) Pisonero, J.; Fernandez, B.; Guenther, D. *Journal of Analytical Atomic Spectrometry* **2009**, *24*, 1145-
375 1160.
- 376 (21) Koch, J.; Guenther, D. *Applied Spectroscopy* **2011**, *65*, 155A-162A.
- 377 (22) Rosenheim, B. E.; Thorrold, S. R.; Roberts, M. L. *Rapid Communications in Mass Spectrometry* **2008**,
378 *22*, 3443-3449.
- 379 (23) Ruff, M.; Wacker, L.; Gaeggeler, H. W.; Suter, M.; Synal, H. A.; Szidat, S. *Radiocarbon* **2007**, *49*, 307-
380 314.
- 381 (24) Fahrni, S. M.; Wacker, L.; Synal, H. A.; Szidat, S. *Nuclear Instruments & Methods in Physics Research*
382 *Section B-Beam Interactions with Materials and Atoms* **2013**, *294*, 320-327.
- 383 (25) Wacker, L.; Muensterer, C.; Hattendorf, B.; Christl, M.; Guenther, D.; Synal, H. A. *Nuclear Instruments*
384 *& Methods in Physics Research Section B-Beam Interactions with Materials and Atoms* **2013**, *294*, 287-290.

- 385 (26) Münsterer, C.; Wacker, L.; Hattendorf, B.; Christl, M.; Koch, J.; Dietiker, R.; Synal, H. A.; Guntherk, D.
386 *Chimia* **2014**, *68*, 215-216.
- 387 (27) Welte, C.; Wacker, L.; Hattendorf, B.; Christl, M.; Koch, J.; Synal, H. A.; Günther, D. *Radiocarbon* **2016**
388 **(in press)**.
- 389 (28) Synal, H. A.; Stocker, M.; Suter, M. *Nuclear Instruments & Methods in Physics Research Section B-Beam*
390 *Interactions with Materials and Atoms* **2007**, *259*, 7-13.
- 391 (29) Wacker, L.; Bonani, G.; Friedrich, M.; Hajdas, I.; Kromer, B.; Nemec, M.; Ruff, M.; Suter, M.; Synal, H.
392 A.; Vockenhuber, C. *Radiocarbon* **2010**, *52*, 252-262.
- 393 (30) Wacker, L.; Christl, M.; Synal, H. A. *Nuclear Instruments & Methods in Physics Research Section B-*
394 *Beam Interactions with Materials and Atoms* **2010**, *268*, 976-979.
- 395 (31) Reimer, P. J.; Brown, T. A.; Reimer, R. W. *Radiocarbon* **2004**, *46*, 1299-1304.
- 396 (32) Gao, P.; Xu, X.; Zhou, L.; Pack, M. A.; Griffin, S.; Santos, G. M.; Southon, J. R.; Liu, K. *Limnol. Oceanogr.*
397 *Meth.* **2014**, *12*, 174-190.
- 398 (33) Fohlmeister, J.; Schroeder-Ritzrau, A.; Scholz, D.; Spoetl, C.; Riechelmann, D. F. C.; Mudelsee, M.;
399 Wackerbarth, A.; Gerdes, A.; Riechelmann, S.; Immenhauser, A.; Richter, D. K.; Mangini, A. *Climate of the*
400 *Past* **2012**, *8*, 1751-1764.
- 401 (34) Farmer, J. R.; Robinson, L. F.; Honisch, B. *Deep-Sea Research Part I-Oceanographic Research Papers*
402 **2015**, *105*, 26-40.

403

404